

### Inventory of Supplemental Information:

Figure S1, related to Figure 1: Figure 1 demonstrates that the orientation tuning properties of cortical cells in adult mice are matched binocularly. Figure S1 further shows that their spatial frequency tuning is also binocularly similar.

Figure S2, related to Figure 2: Figure 2 examines the degree of binocular matching of orientation preference during development. In support of the main figure, Figure S2A further shows the raw data of orientation preference correlation throughout development. Figure S2B-C are important control data demonstrating that the orientation preference obtained in our experiments are similarly reliable in both young and adult mice.

Figure S3, related to Figure 4: Figure S3 raises the possibility that the development of binocular matching of orientation preference might be due to an increase in orientation selectivity, as less selective cells appeared to have slightly larger  $\Delta O$ . Figure 4 rules out this possibility by examining the monocular features of orientation tuning during development.

## Supplemental Figures

Figure S1

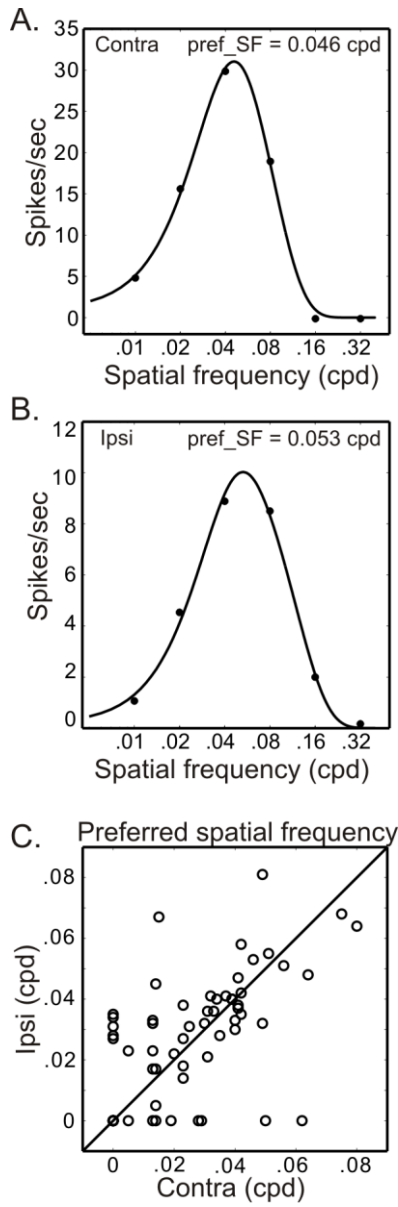


Figure S1, related to Figure 1, Binocularly similar spatial frequency tuning in adult mice.

(A and B) Spatial frequency tuning curves of a binocular cell with similar preferred spatial frequency through the two eyes. (C) Correlation of preferred spatial frequency through the two eyes in adult mice ( $r = 0.43$ ,  $P < 0.001$ ,  $n = 61$ ). Preferred spatial frequency of the cells with low-pass responses were represented as 0 cpd.

Figure S2

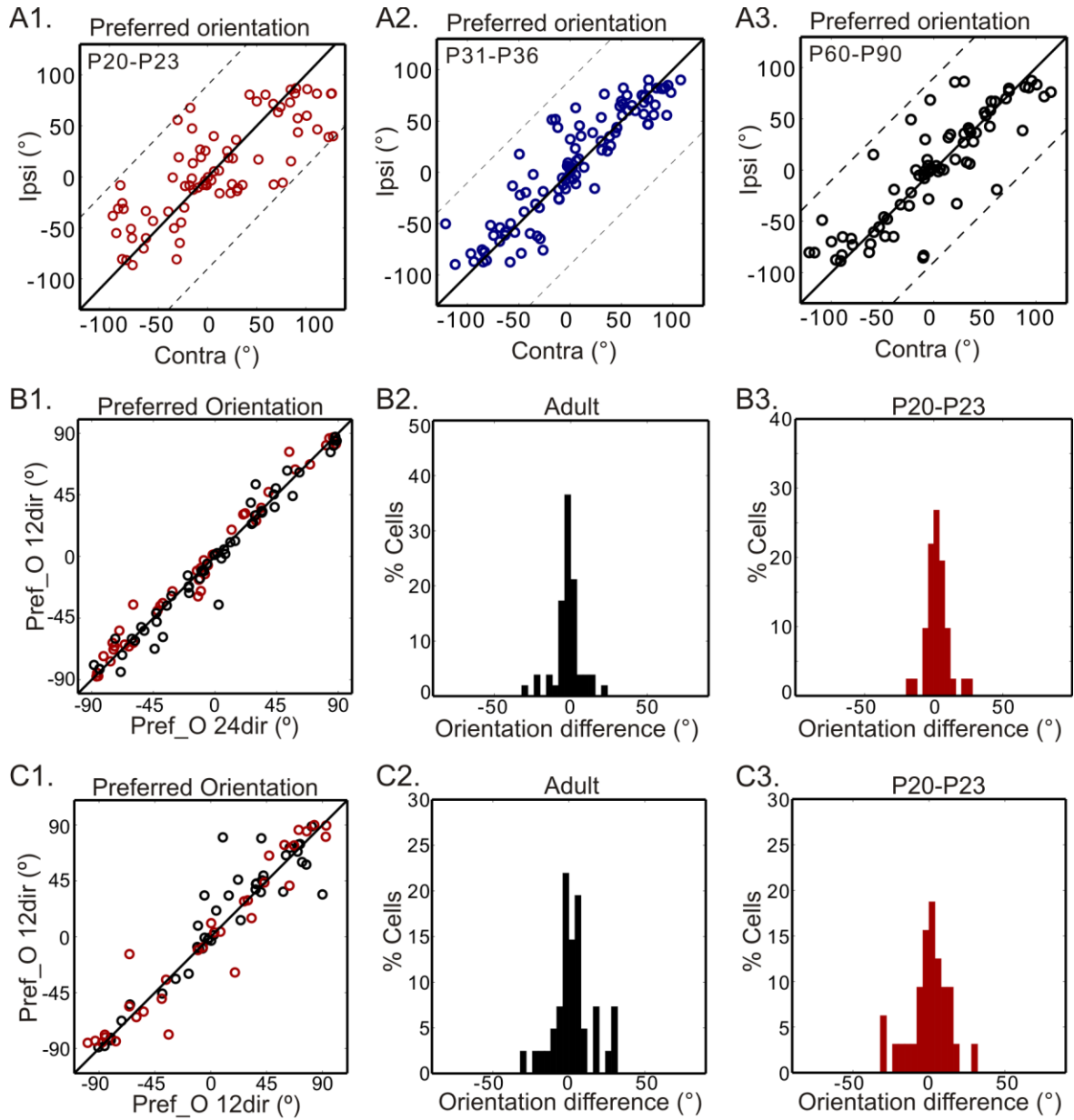


Figure S2, related to Figure 2: Development of binocular correlation of orientation preference.

(A) Correlation of contralateral (x axis) and ipsilateral (y axis) orientation preference for P20-P23 (A1,  $r = 0.80$ ,  $P < 0.0001$ ,  $n = 80$ ), P31-P36 (A2,  $r = 0.91$ ,  $P < 0.0001$ ,  $n = 100$ ) and P60-P90 (A3,  $r = 0.86$ ,  $P < 0.0001$ ,  $n = 75$ ) mice. The dotted lines bound the region in which the data points can lie. Panel A3 is reproduced from Figure 1C for direct comparison across ages. Note that the correlation is “wider” in P20-23 mice.

(B) Preferred orientations obtained with drifting gratings of 12 directions ( $30^\circ$  steps) or 24 directions ( $15^\circ$  steps) in the same cells were nearly identical (adult: black circles,  $r = 0.98$ ,  $P < 0.0001$ ,  $n = 52$ ; P20-P23: red circles,  $r = 0.98$ ,  $P < 0.0001$ ,  $n = 41$ ). (B2-B3) The difference between the preferred orientations obtained from the two ways of analyses was similarly small in adult (B2, mean =  $5.9^\circ \pm 1.0^\circ$ ) and P20-P23 mice (B3, mean =  $5.9^\circ \pm 0.9^\circ$ ).

(C) Similar orientation preference were obtained when repeating the 12-direction drifting grating stimuli (adult: black circles,  $r = 0.93$ ,  $P < 0.0001$ ,  $n = 41$ ; P20-P23: red circles,  $r = 0.96$ ,  $P < 0.0001$ ,  $n = 32$ ). (C2-C3) The orientation difference between the two full series were similarly small in adult (C2, mean =  $11.4^\circ \pm 2.4^\circ$ ) and P20-P23 mice (C3, mean =  $11.4^\circ \pm 2.4^\circ$ ). The results in panels B and C demonstrate reliable measurement of preferred orientations in both young and adult mice.

Figure S3

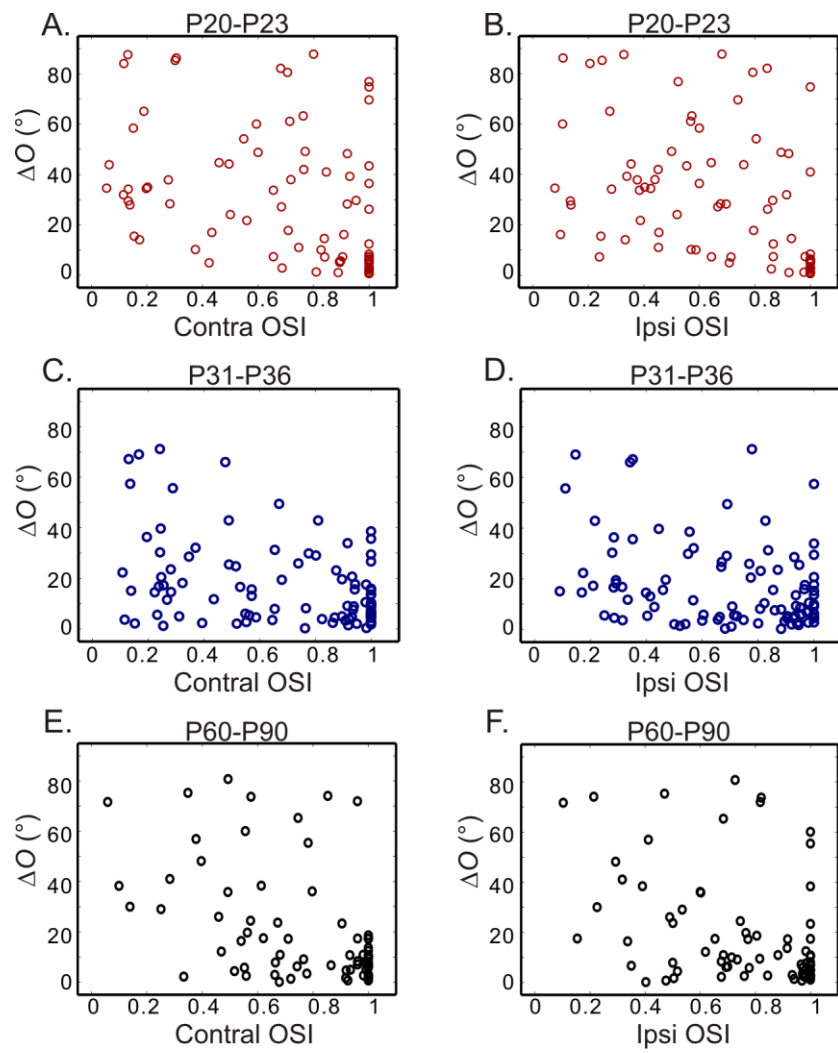


Figure S3, related to Figure 4: Scatter plots of  $\Delta O$  vs. contralateral (A, C, E) or ipsilateral OSI (B, D, F) through development, at P20-P23 (A and B), P31-P36 (C and D), and P60-P90 (E and F).

Note that less selective cells appear to have slightly larger  $\Delta O$ , though large  $\Delta O$  can occur throughout the whole range of OSI in all panels.